

## Three dimensional visualization of histopathological data

**Aleksandra Podwójcik**

Centre of Informatics – Tricity Academic Supercomputer Network (CI TASK)

Gdansk University of Technology

Gabriela Narutowicza 11/12, 80-233 Gdansk

<https://doi.org/10.34808/6cw9-7j22>

### Abstract

The histopathological examination provides information about the spatial assessment of pathological changes in the tissue. The authors present a method of extending this histopathological spatial assessment with a 3D view consisting of images of microscopic layers. The proposed solution creates 3D models based on images obtained from the database of the Medical University of Gdańsk (Digital Pathology). First, a series of medical images related to the study of a specific pathological tissue undergoes a process of background detection and removal through an algorithm. Next, images are aligned with each other. Then, two types of 3D models are created: 1) classical model with Marching Cubes algorithm and 2) the use of Cloud of Points.

### Keywords:

Histopathology, DICOM, Digital Pathology, 3D models

# 1. Introduction

Histopathology is a field that deals with analysis of microscopic phenomena occurring in tissues associated with various types of diseases. In the traditional approach, the pathologist, during the histopathological examination, evaluates the condition of the tissue by observing it under a microscope and makes a diagnosis. Today, thanks to the digitization process, it is possible to create digital tissue images and use them for diagnosis.

The Center of Informatics Tricity Academic Super-computer and Network (CI TASK), together with the Medical University of Gdańsk (MUG), has created a Digital Pathology (DP) database which provides a repository service and a 2D DICOM viewer [1]. The authors plan to improve their work by creating a new viewer that would enable clinicians to analyze histopathological samples using 3D models. For this purpose, a review of the literature was carried out to find solutions that would correspond to the presented problem.

One significant observation from the articles is that many of the models rely on images from Computed Tomography or Magnetic Resonance Imaging. Due to the information about the position of the pixels and spacing between slices, the DICOM format can be used directly to build 3D models (e.g. Pydicom [2]) [3]. In the case of histopathological images, such parameters are not available in DICOM files, so there is a need to perform many more steps to match the individual images that make up a 3D model. Images from Computed Tomography or Magnetic Resonance have the additional property that they are presented in an HU unit [4, 5], thanks to which, after setting the appropriate threshold, it is possible to easily separate the organ area from the background, which is not so easy in the case of histopathological images. Many solutions rely on pre-existing software to manually generate 3D models [6, 7, 8]. This approach has limitations as it requires a particular set of skills in 3D modeling. The DP is quite a large and diverse data set, which makes it practically impossible to use a manual approach, especially since the main goal is to add the functionality of creating a 3D model to the DP application.

Therefore, the main goal will be to create a solution that will generate the model automatically, omitting the background and recreating spatial relationships between individual parts.

## 1.1. Digital Pathology Workflow

There are two sources of material for histopathological examination stored in the DP database: tissues collected during surgery by surgeons from the University Clinical Center in Gdańsk and tissues from archives of

Pathology Departments. In the case of tissues taken from surgery, the next step is tissue fixation. Fresh tissue material is fixed in a 4% formaldehyde water solution (10% neutral buffered formalin). Fixation preserves the structure of living cells. After fixation, the tissues undergo processing to make them suitable for slicing (creating paraffin blocks from tissues) and then embedding and machining [1]. The final stage of tissue preparation is its staining, without which the image would be illegible and ambiguous [1]. In a digital approach, special equipment is used to obtain images of tissue samples. The principle of operation of histopathological scanners is based on a combination of the functions of an optical microscope and a digital camera. The camera mounted in the scanner can record the image from the entire slide using selected magnification or autofocus functions. The following cameras are used in the Department of Medical Laboratory Diagnostics at the MUG: Pannoramic 250 III Flash 3DHitech and Olympus VS200. Prior to scanning, sets of histological slides are registered in the local IT system, which is the baseline database. Histological and cytological preparations registered in the local IT system are scanned to obtain their digital record. Files range from about 1 GB to even 30 GB in size. Images acquired in native *mrxs* or *vsi* formats are converted to a DICOM file [1]. DICOM (Digital Imaging and Communications in Medicine) is the standard used to unify and exchange medical data associated with images. The DICOM format is suitable for storing large format data [9]. Thanks to DICOM it is possible to send medical photos while maintaining their good quality and other medical data related to the examination.

## 1.2. Digital Pathology

MUG has created an open image database (Digital Atlas of Tissues and Cells): a rich and varied collection of digital images of histological and cytological preparations developed for building the repository. The DP platform provides a means for accessing and analyzing the data [1]. The medical data provided by DP is approved and described by MUG pathology specialists and made public, along with the necessary metadata. This app provides a chance to view, for free, high-quality images along with unique clinical data in an anonymous way.

# 2. Materials and methods

## 2.1. Background removal

There are many tissue images available in the Digital Pathology application. At this moment, twenty four images of appendix tissues were selected for the creation of

3D models. The first step in creating these models was to remove the background from the images.

The Digital Pathology repository mentioned earlier provides JPEG images exported from selected views of their DICOM counterparts. Due to the nature of the process of scanning samples e.g. cutting and subsequent deformation or artificial light emitted by the scanner, these images often contain a series of artifacts (Fig. 1). These often include uneven background coloring and outlining pixels representing a shredded tissue disconnected from a sample. The authors should use a removal method to remove such artifacts to obtain high-quality 3D models. Currently, the backgrounds only are removed for fear of distorting the images. A different algorithm will need to be developed in the future to eliminate any remaining artifacts. The first step to remove the background is to convert a three-channel (RGB) image to a four-channel (RGBA) image, where the alpha component is responsible for the pixel transparency (a pixel with an alpha value of 0 is completely transparent). The next step is to find the threshold value above which the pixel value of alpha and other channels will be set to zero.

In this case, authors used two thresholds: Otsu's method threshold [10] and second one that relies on the vector of the pixels' values frequency. The hypothesis confirmed by empirical research is that about 0.3% of the highest and most frequently occurring values make up the background. The remaining pixel values of the image (99.7%) correspond to three times the standard deviation of the frequency vector value. Therefore, this value can be used to determine the threshold above which background pixels can be removed.

Here is the pattern used to filter out the background pixels.

$$(FT * BR) + (OT * (1 - BR)) = BT \quad (1)$$

*BT* - Background Threshold

*FT* - Frequency Threshold

*OT* - Otsu Threshold

*BR* - Blend Ratio, values  $\in \langle 0, 1 \rangle$

Fig. 1 presents an example image of the appendix, before (a) and after (b) background removal.

## 2.2. Image registration

The selected images show consecutive tissue fragments from the same organ. The cut caused a loss of spatial relationship between the tissues. It was necessary to match the images and recover the spatial relationships to create a 3D model of the entire organ. The authors used a selected group of image alignment methods to recover the said spatial relationship.

The first method was homography [11]. The homography is a  $3 \times 3$  matrix (Eq. 2) that represents a transformation of coordinates of a pixel in one image to its corresponding position in another image.

$$H = \begin{bmatrix} h_{00} & h_{01} & h_{02} \\ h_{10} & h_{11} & h_{12} \\ h_{20} & h_{21} & h_{22} \end{bmatrix} \quad (2)$$

The method involves identifying the key points in both the compared images, with one serving as a template. The ORB algorithm [12] indicates the key points and their descriptors. Next, the Hamming method [13] calculates the distance between binary features to find the best matches. It is the pixel pairs with the smallest distances only that are kept. The rest are ignored (Fig. 2).

The selected key points and the RANSAC [14] algorithm are used to calculate the homography matrix. The homography matrix transforms the target image. The aligned image is used as a reference image for the alignment of the next one. Fig. 3 presents the effects of the described alignment method.

The other methods tested in this paper come from the `pystackreg` Python library [15]. The first group of methods implemented is based on alignment concerning the reference image and includes: translation (Fig. 4), rigid body (Fig. 5), scaled rotation (Fig. 6), affine (Fig. 7) and bilinear (Fig. 8)

The second group of the implemented methods is based on the transformation of the entire image stack by the adopted algorithms. These are the alignments: according to the first image in the stack (Fig. 9), according to the previous image (Fig. 10), according to the average of the images in the stack (Fig. 11), according to the average of the first  $n$  images (Fig. 12), according to the moving average of the  $n$  images (Fig. 13).

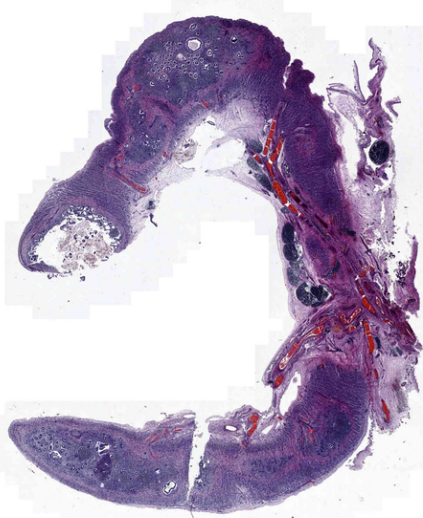
## 2.3. Canny filtration

The best way to check the operation of the alignment algorithm is to put all the twenty four selected aligned images in one image and see how they fit together. An image consisting of many other images loses legibility. Therefore, before combining them, they should be subjected to feature reduction. In this case, the Canny filtration [16] can be used to reduce features.

The Canny filter extracts only the outlines from the image. These outlines are originally white. There was a need to color them to increase visibility. The contours were colored in two ways, first with a random color and then with a color map (the more pixels in the image, the bluer the contour was). Fig. 14 shows the Canny filtration result with colored contours for the twenty four selected and not aligned appendix images.



(a)



(b)

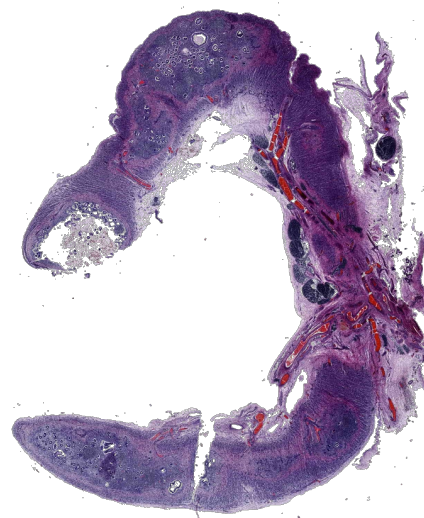


**Figure 1:** Comparison of two images, with (a) and without (b) background

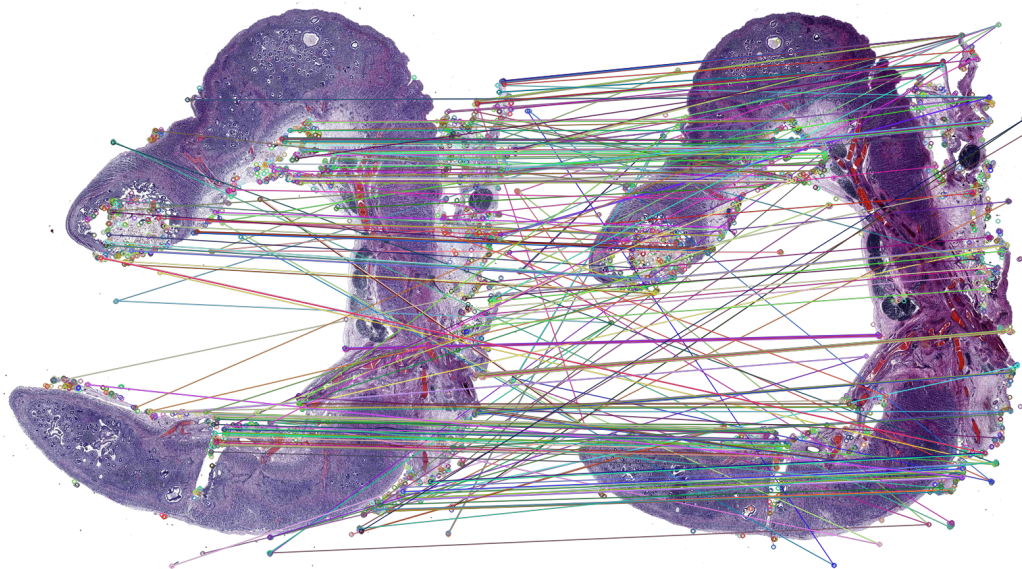
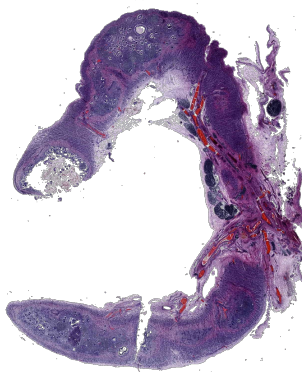
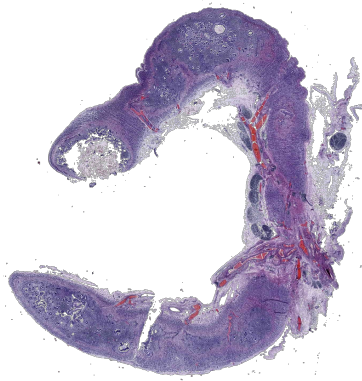


**Figure 2:** Key points are selected by a combination of the Hamming method and the ORB algorithm, with the distances shown for each pair of pixels from the two selected appendix images

(a)



(b)



(c)

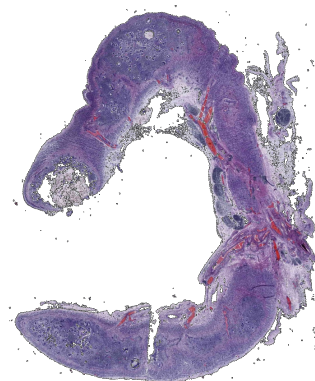


**Figure 3:** Comparison of three appendix images: reference (a), unaligned (b) and aligned (c) with the homography method



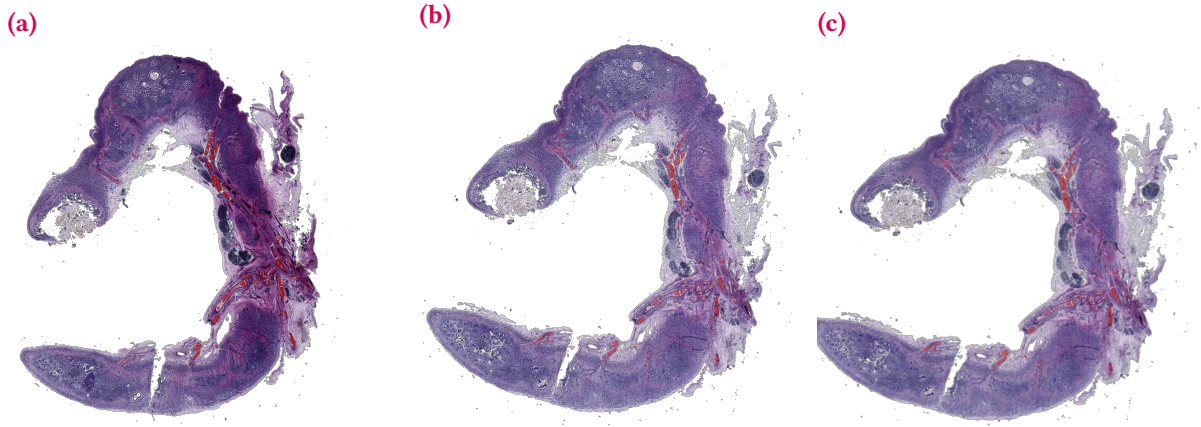


**Figure 4:** Comparison of three appendix images: reference (a), unaligned (b) and aligned (c) with translation transformation

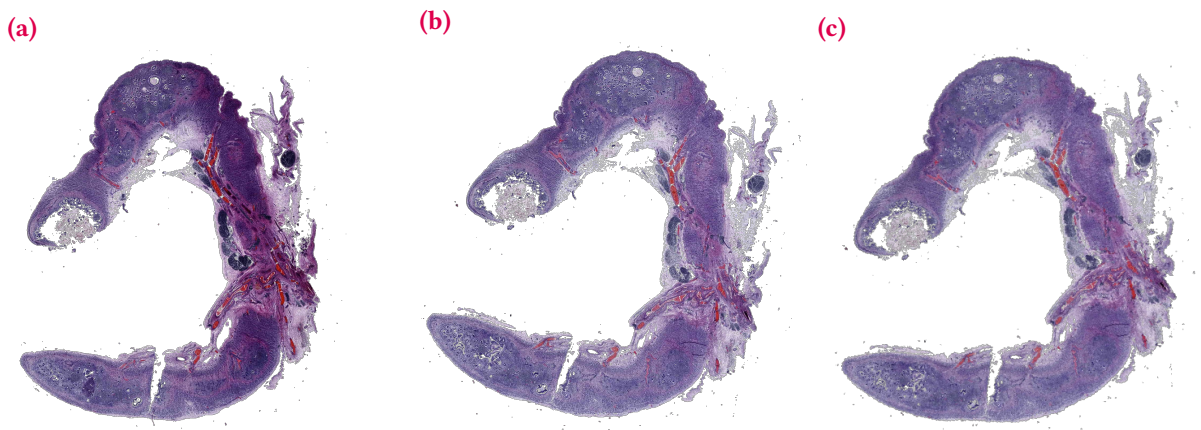


**Figure 5:** Comparison of three appendix images: reference (a), unaligned (b) and aligned (c) with rigid body transformation

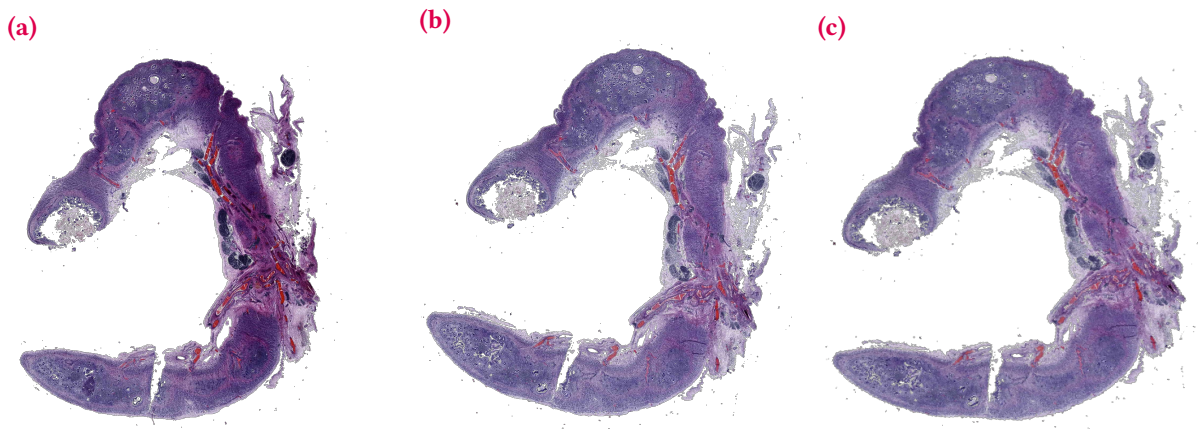


**Figure 6:** Comparison of three appendix images: reference (a), unaligned (b) and aligned (c) with scaled rotation transformation

These visualizations were also created for each of the alignment methods. The result was that the best-fit method was an affine transformation from the `pystack-reg` library. Fig. 15 shows the contours of the Canny filter after the affine transformation.

## 2.4. Creation of 3D model

3D models of histopathological samples were prepared based on the images processed with the aforementioned alignment methods.

The first method used is based on the Marching Cube algorithm [17]. The Background removal process provides information about which pixels belong to the sample and which belong to the background. This means

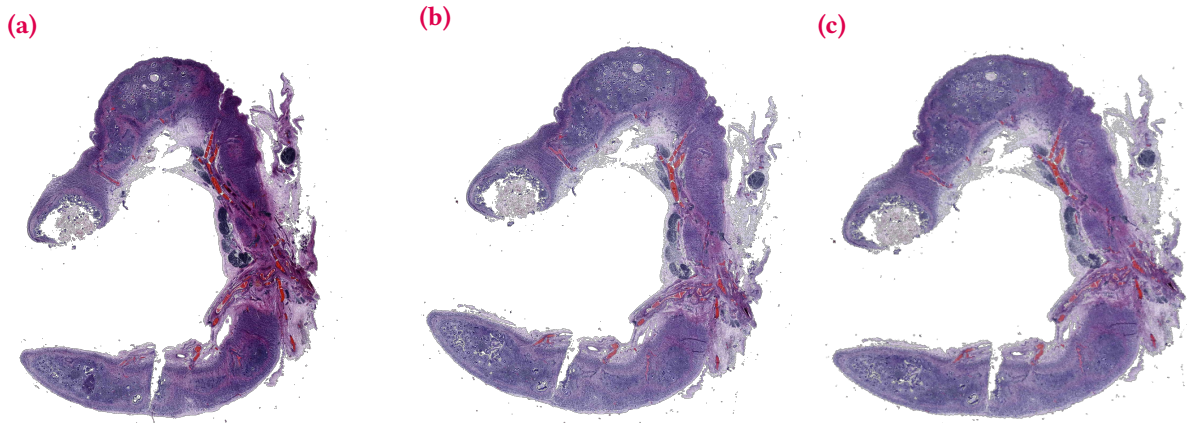


**Figure 7:** Comparison of three appendix images: reference (a), unaligned (b) and aligned (c) with affine transformation

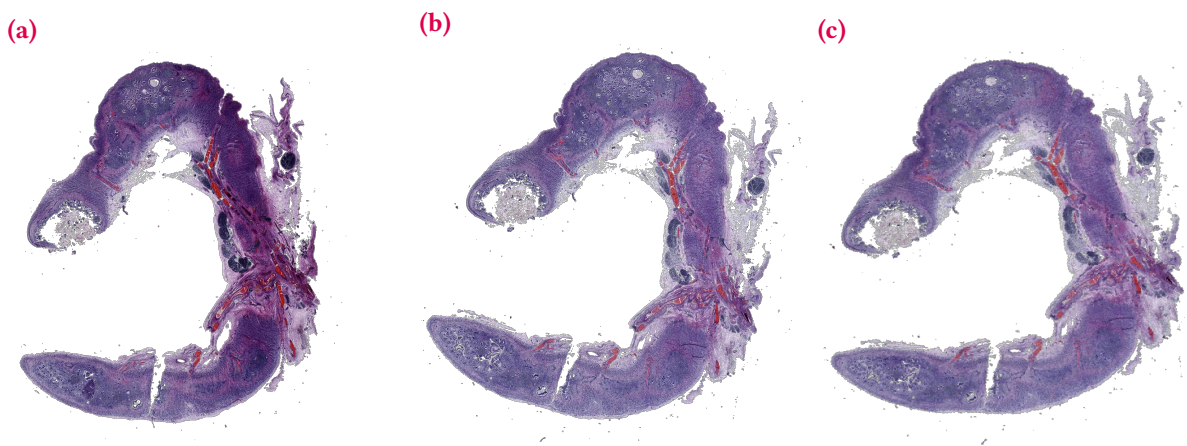


**Figure 8:** Comparison of three appendix images: reference (a), unaligned (b) and aligned (c) with bilinear transformation

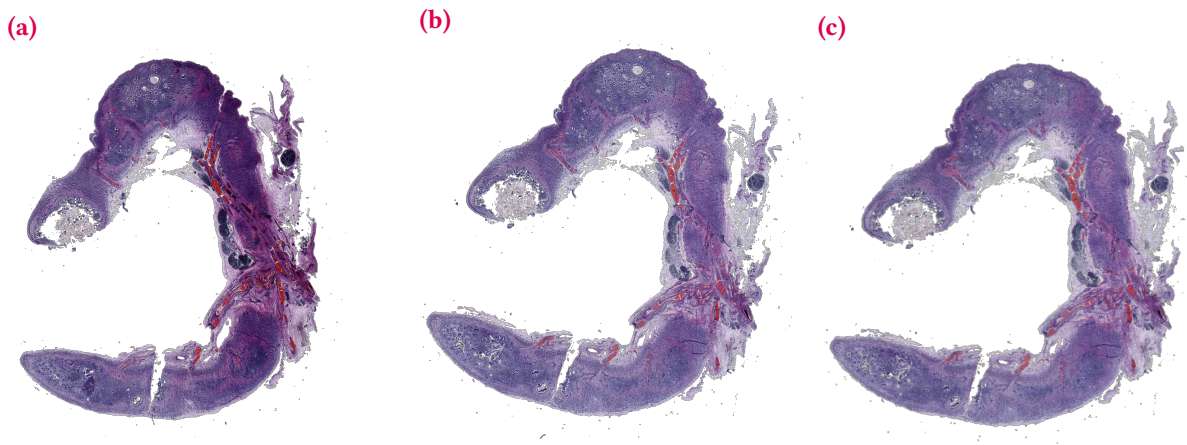


**Figure 9:** Comparison of three appendix images: first stack image (a), second unaligned stack image (b) and aligned version of this image (c) aligned according to first stack image

that it is feasible to create "3D pixels," also known as voxels, by selecting a pixel and its neighboring pixels. A voxel is a cube defined by pixel values in its corners, enabling the use of the Marching Cube method. If one or more pixels have a value smaller than the user-specified isovalue (threshold), and one or more have values greater than this value, the voxel must contribute some isosurface component. Triangular patches that divide the cube can

be created between regions within the isosurface and regions outside by specifying which edges of the cube are intersected by the isosurface. Combined patches from all of the constructed cubes at the boundary of the isosurface give an approximate representation of the sample surface. In this way, a solid can be obtained from a 2D image using this approach. The model represents the boundary of a given image only, i.e. its shell (Fig. 16a). Due to this,



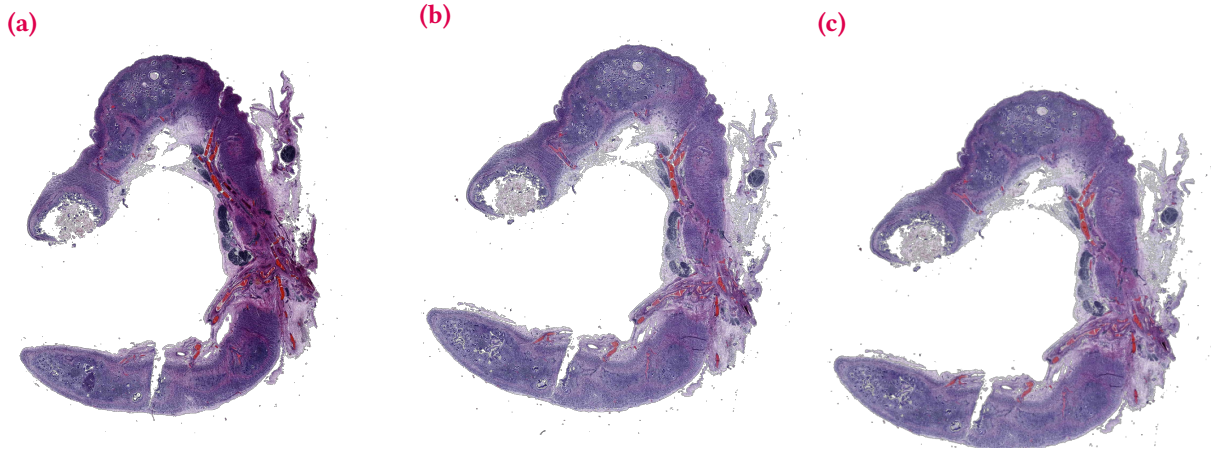


**Figure 10:** Comparison of three appendix images: previous stack image (a), next unaligned stack image (b) and aligned version of this image (c) aligned according to the previous stack image

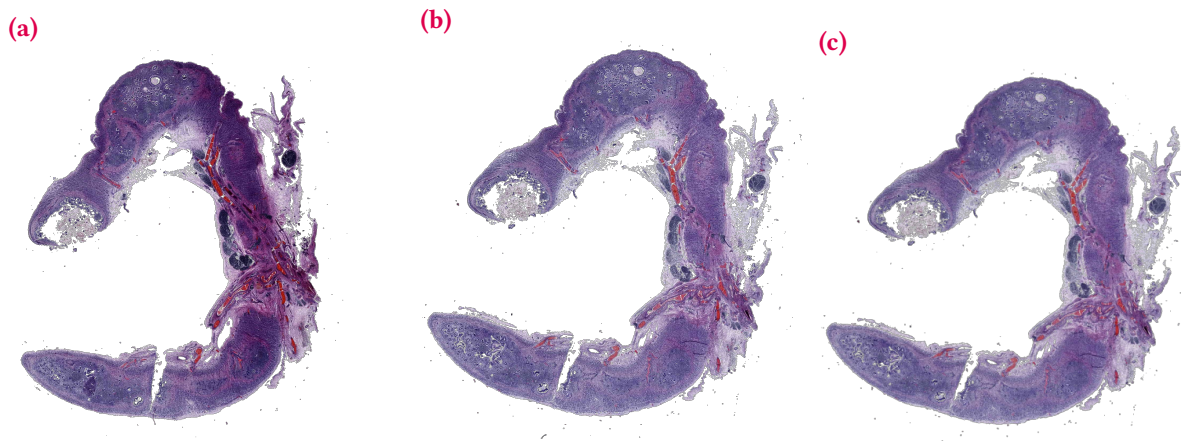


**Figure 11:** Comparison of two appendix images: unaligned (a) and aligned (b) with the image transformation average

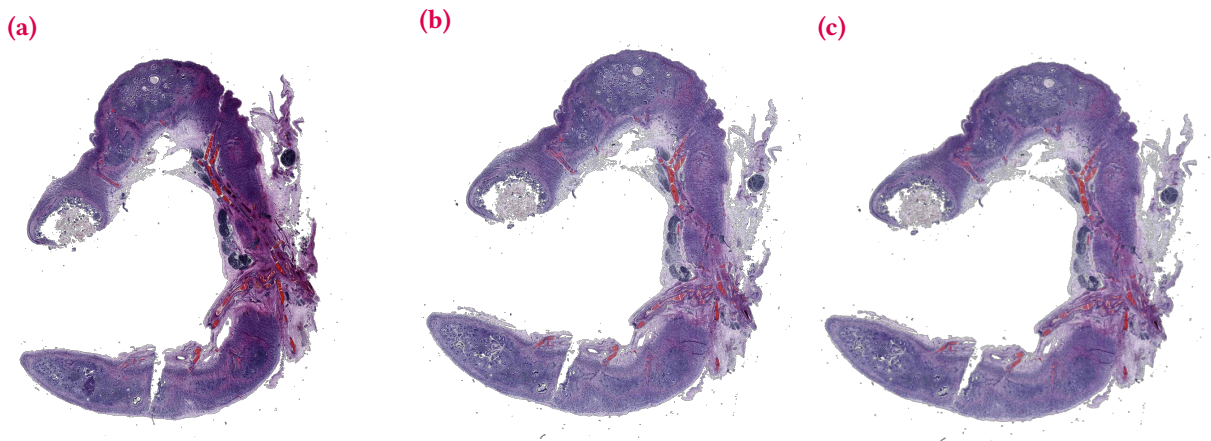


**Figure 12:** Comparison of two appendix images: unaligned (a) and aligned (b) with the average of the first transformation of  $n$  images (in this example  $n$  is equal to 10)

additional top and bottom layers have to be constructed using their corresponding DICOM scans (Fig. 16b).

The Fig. 17 shows the final model, consisting of twenty-four component solids for each layer.

Fig. 17 shows the final model consisting of twenty four component solids for each layer.

In the second method, based on the analyzed images,

a matrix of points corresponding to the spatial location of pixels is created. This data was used to build a 3D model, where the position of each pixel is represented by a cube to which the color corresponding to that pixel is assigned. As in the first method, the images intended for building the model are aligned and have the background removed.

The source images of the tissue scans used to build



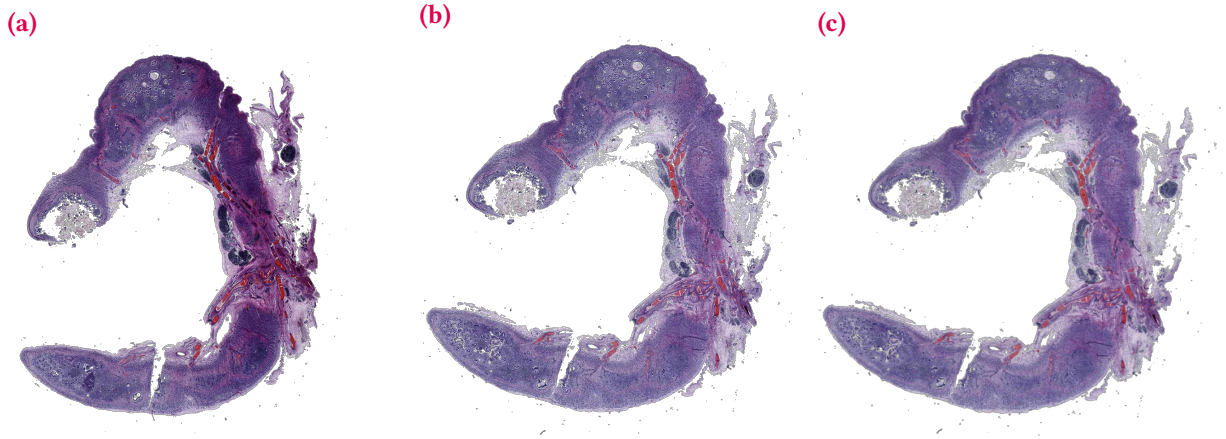


**Figure 13:** Comparison of two appendix images: unaligned (a) and aligned (b) with the moving average of the transformation of  $n$  images (in this example  $n$  is equal to 10)

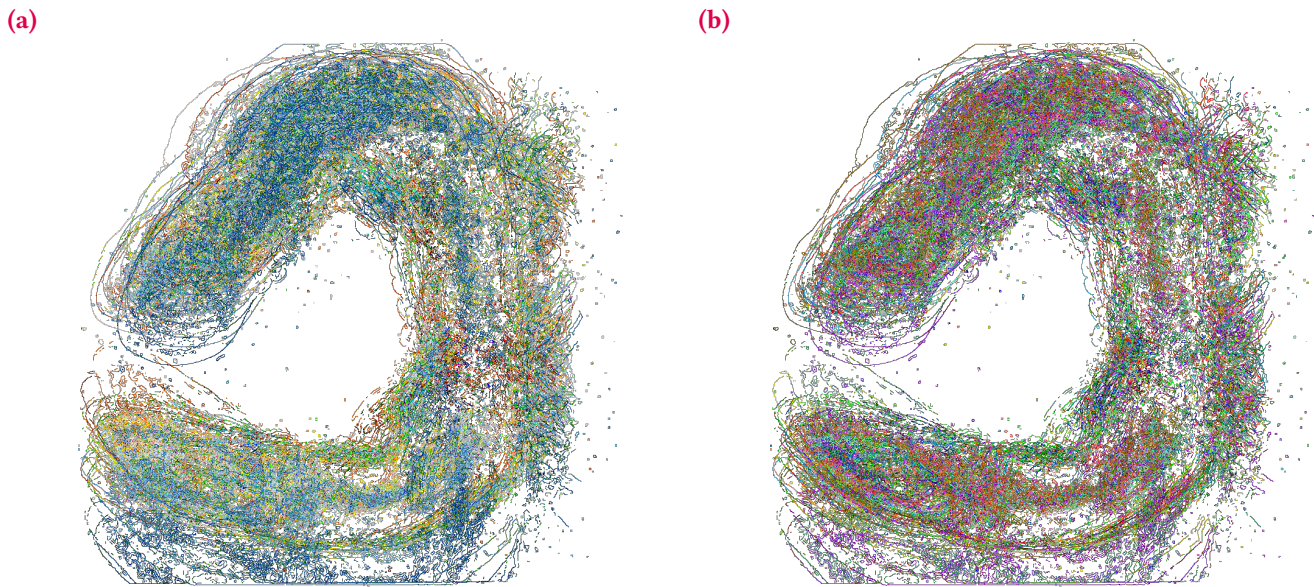


**Figure 14:** Contours of unmatched images colored with selected colors (a) or with colors from the color map (b)

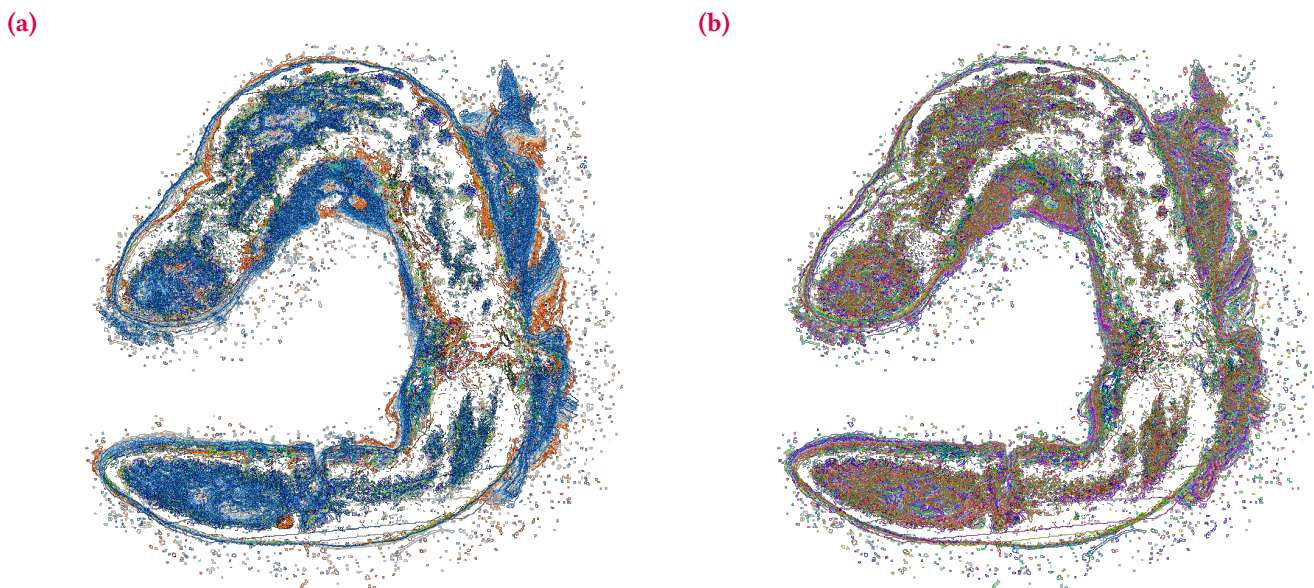
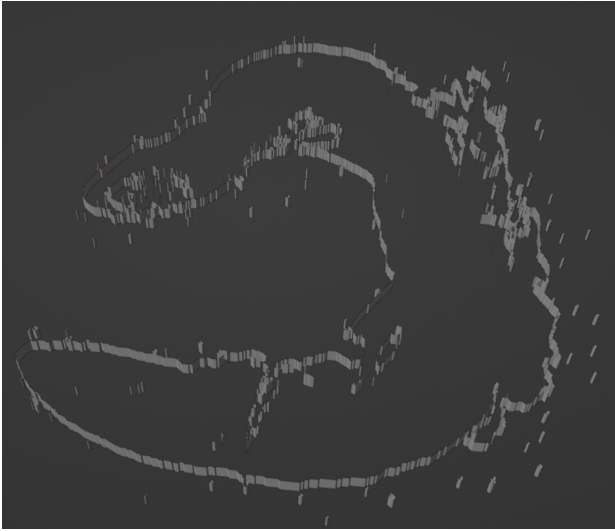


**Figure 15:** Contours of matched images after affine transformation, colored with selected colors (a) or colors from the color map (b). This visualization demonstrates the significance of accurately matching images in order to create a complete 3D model of an organ

(a)



(b)



**Figure 16:** A 3D model created from a 2D image

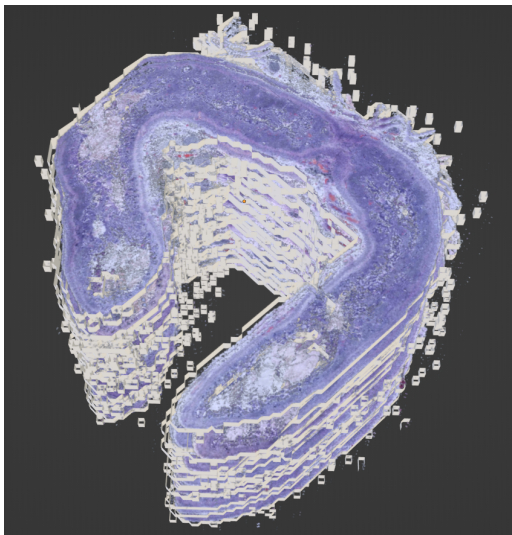


**Figure 17:** The 3D model consisting of twenty four layers. Each layer was created from an image with the background removed and the affine transformation aligned

the 3D model are 8-bit .jpg files in which more than 16 million colors can theoretically occur. Therefore, a very important step is to convert the colors to a limited number. With a relatively small number of colors (relative to the source tissue scans), it is possible to group the cubes based on their colors and easily switch them from a visible to invisible mode and vice versa, increasing the readability of areas of interest in the tissue model. The image in Fig. 18 displays the appendix using a palette of only 24 colors, which was chosen based on empirical data.

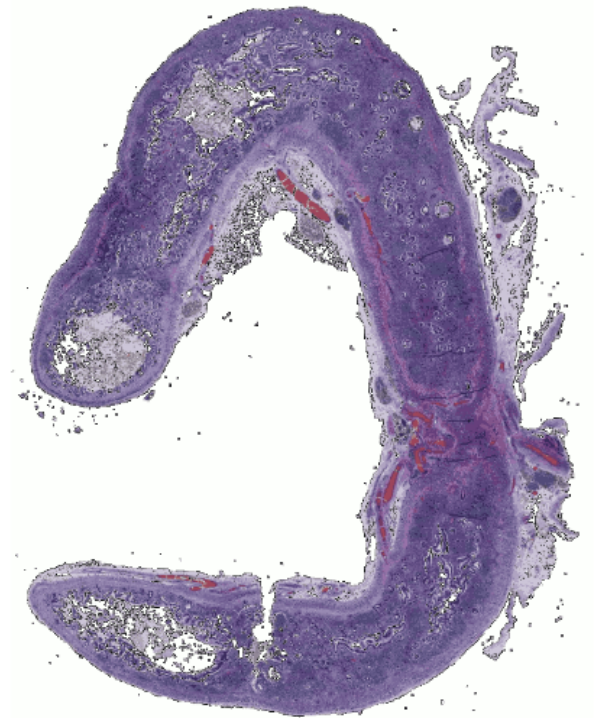


**Figure 18:** Image of an appendix reduced to twenty four colors

Fig. 19 shows different versions of the 3D model made with the method described. The models have specific colored pixels turned on.



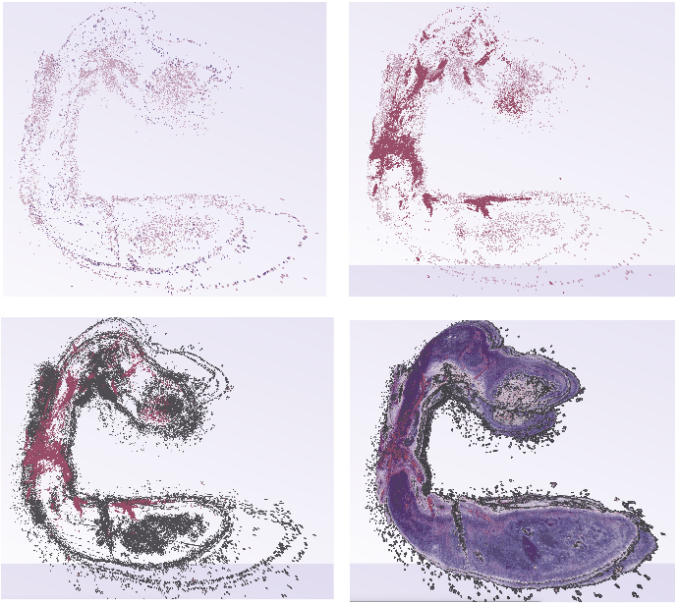


**Figure 19:** 3D models of an appendix are created following the previously mentioned process

## 2.5. The computational complexity of the process of creating a 3D model

A computational complexity analysis was performed for the process of creating a model using the Marching Cube algorithm. This complexity was examined using two aspects: time and memory consumption. Fig. 20 presents charts showing changes in the number of these two resources depending on the changing number of images from which the models are built.

The execution time of the program increases exponentially with the amount of the input data. This is not a desirable phenomenon because as the amount of data increases, the algorithm becomes ineffective and impractical. In the future, changes should be made to the scripts to make this time as short as possible when handling increasingly larger data sets.

In the case of memory, the situation is much better because the consumption graph is near logarithmic, which means that the increasing amount of data does not significantly affect the memory consumption.

## 3. Conclusions

The solutions presented in the article are the first steps in the development of methods for creating 3D models of organs from DICOM images. The main advantages of the presented solutions are the use of free technologies such as Blender or Three.js, the use of the Python library to automatically create models, effective techniques for removing the background and aligning images.

The article includes a section about filtering images to remove unwanted fragments that could affect the structure of a 3D model. It presents a formula that can eliminate background pixels. However, small pieces of tissue remain a problem and need to be removed as well. Therefore, in the future, there will be a need to improve the current algorithm or use a new one to remove these artifacts.

The section on image alignment presents the results of changes in the position and orientation of sample images relative to the reference image, obtained for the homography method and alignment methods from the `pystackreg` library. The use of Canny filtering helped identify the most suitable algorithm for aligning images of appendix tissues. It is possible to combine different methods for better results. For instance, the alignment method from the `pystackreg` library can be applied to an image, followed by applying the homography method to the same image, or vice versa. It would be beneficial to explore the outcomes of such combinations in future studies. In addition, since the effectiveness of matching algorithms may vary depending on the tissue under consideration, it is advisable to develop an algorithm that would produce a numerical result rather than a visual one.

Three-dimensional tissue models were created using two methods: Marching Cubes and Matrix Of Points. The presented models were created from images with a resolution of  $500 \times 500$  pixels. These and similar dimensions are sufficient for the purpose of experimental determination of individual steps in creating a 3D model. However, in the long term, models should be created from images with a higher resolution, for example, 40.000 pixels. In the future, there will be a need to use distributed rendering of 3D models to be able to create a model from such large images. The program should also be improved in terms of time complexity so that the increased amount of data should not result in too long waiting times for the effect while maintaining low memory consumption.

In summary, the main goal is to develop a method or a set of methods that would allow the creation of the most accurate 3D models with a high resolution, regardless of the type of tissue provided by the Digital Pathology database.

## Acknowledgements

Computations were carried out using the computers of Center of Informatics Tricity Academic Supercomputer & Network.



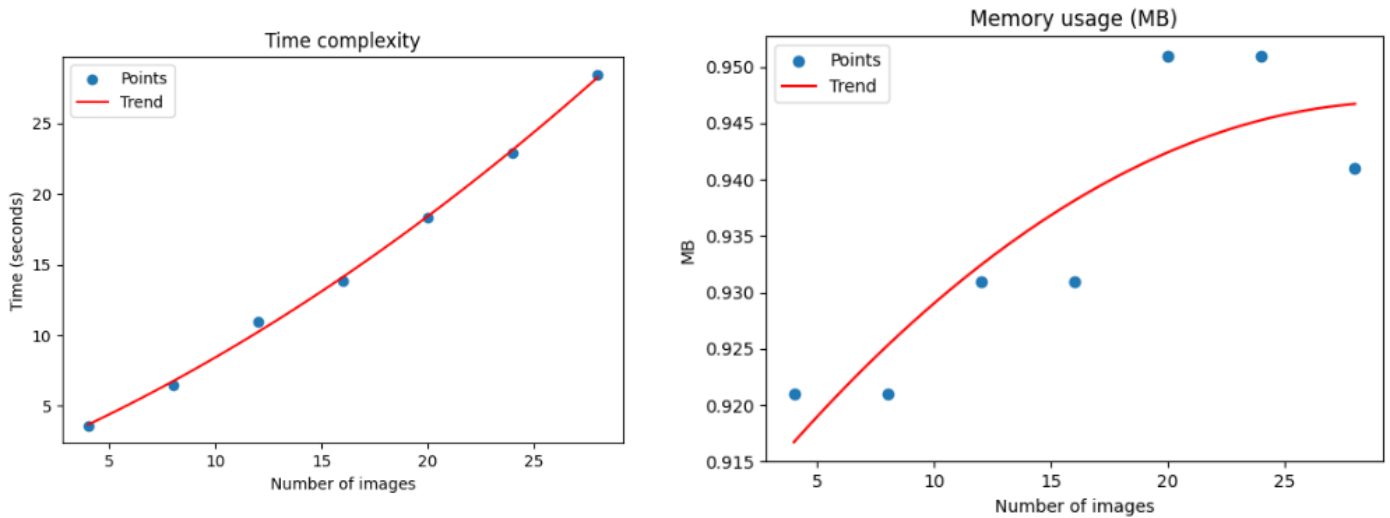


**Figure 20:** Charts showing changes in the amount of a) time b) and memory used depending on the number of images used to build models. Due to limited technical capabilities, the number of images used to build the model was limited to twenty eight, which made it necessary to use a trend line chart

## References

- [1] M. Bolcewicz, J. Gulczyński, K. Jendernalik, L. Kalinowski, A. Lewandowska, J. Skokowski, and T. van de Wetering, "The digital tissue and cell atlas and the virtual microscope," *Sharing research data across disciplines*, vol. 1, pp. 61–69, 01 2022.
- [2] D. Mason and contributors, "pydicom: DICOM for Python." <https://pydicom.github.io/pydicom/stable/>, 2023. Accessed: 02.06.2023.
- [3] H. R. Gamba, P. Nohama, A. A. C. Paz, I. J. Sanches, and M. A. Souza, "3d thermal medical image visualization tool: Integration between MRI and thermographic images," in *36th Annual International Conference of the IEEE Engineering in Medicine and Biology Society*, pp. s. 61–64, IEEE, 08 2014.
- [4] J. Cychnerski, K. Kaczor, A. Kwaśniewska, P. Nadachowski, M. Operlejn, A. Piastowski, and M. Zielonka, "Comparison of image pre-processing methods in liver segmentation task," in *15th International Conference on Human System Interaction (HSI)*, pp. s. 1–6, IEEE, 07 2022.
- [5] F. Wang, J. Zhang, and Q. Xue, "A human neck finite element model basing on DICOM data," in *2009 3rd International Conference on Bioinformatics and Biomedical Engineering*, pp. s. 1–4, IEEE, 06 2009.
- [6] F. Pu, D. Jin, S. Li, D. Li, H. Niu, Y. Yang, and Y. Fan, "Reconstruction of three-dimensional model of normal female pelvic cavity based on magnetic resonance imaging," in *2007 IEEE/ICME International Conference on Complex Medical Engineering*, pp. 732–735, 2007.
- [7] V. Simic, M. Milosevic, I. Saveljic, B. Milicevic, N. Filipovic, and M. Kojic, "3D reconstruction and computational modeling of solid-fluid interaction in realistic heart model," in *BIBE 2021 - 21st IEEE International Conference on BioInformatics and BioEngineering, Proceedings*, BIBE 2021 - 21st IEEE International Conference on BioInformatics and BioEngineering, Proceedings, (United States), Institute of Electrical and Electronics Engineers Inc., 2021.
- [8] P. Valchanov and S. Pavlov, "High fidelity anthropomorphic 3D printed models - accuracy, precision and quality control," pp. 1–4, 11 2022.
- [9] DICOM Standards Committee, "DICOM standard." <https://www.dicomstandard.org/>, 2023. Accessed: 16.05.2023.
- [10] N. Otsu, "A threshold selection method from gray-level histograms," *IEEE Transactions on Systems, Man, and Cybernetics*, vol. 9, no. 1, pp. 62–66, 1979.
- [11] R. Hartley and A. Zisserman, *Multiple View Geometry in Computer Vision*. Cambridge University Press, 2 ed., 2003.
- [12] E. Rublee, V. Rabaud, K. Konolige, and G. Bradski, "ORB: An efficient alternative to SIFT or SURF," in *2011 International Conference on Computer Vision*, pp. 2564–2571, 2011.
- [13] R. W. Hamming, "Error detecting and error correcting codes," *The Bell System Technical Journal*, vol. 29, no. 2, pp. 147–160, 1950.
- [14] R. C. Bolles and M. A. Fischler, "Random sample consensus: a paradigm for model fitting with applications to image analysis and automated cartography," *Communications of the ACM*, vol. 24, no. 6, pp. 381–395, 1981.
- [15] P. Thévenaz, U. E. Ruttimann, and M. Unser, "A pyramid approach to subpixel registration based on intensity," *IEEE Transactions on Image Processing*, vol. 7, no. 1, pp. 27–41, 1998.
- [16] J. F. Canny, "A computational approach to edge detection," *IEEE Transactions on Pattern Analysis and Machine Intelligence*, vol. 8, no. 6, pp. 679–698, 1986.
- [17] H. E. Cline, W. E. Lorensen, S. Ludke, C. R. Crawford, B. C. Teeter, J. W. Hetrick, R. A. Schachar, D. P. Greenberg, C. R. Volpe, J. W. Philbrick, *et al.*, "Two algorithms for the three-dimensional reconstruction of tomograms," *Computer Graphics*, vol. 21, no. 4, pp. 163–169, 1987.